sciendo

DOI 10. 2478/ama-2021-0016

acta mechanica et automatica, vol.15 no.3 (2021)

MATHEMATICAL MODELLING OF WATER-BASED Fe_3O_4 NANOFLUID DUE TO ROTATING DISC AND COMPARISON WITH SIMILARITY SOLUTION

Anupam BHANDARI*

*Department of Mathematics, School of Engineering, University of Petroleum & Energy Studies (UPES), Energy Acres Building, Bidholi, Dehradun- 248007, Uttarakhand, India

pankaj.anupam6@gmail.com

received 8 July 2020, revised 6 June 2021, accepted 15 June 2021

Abstract: The current research demonstrates the revolving flow of water-based Fe_3O_4 nanofluid due to the uniform rotation of the disc. This flow of nanofluid is investigated using CFD Module in COMSOL Multiphysics. However, the similarity solution for this flow is also obtained after transforming the given equation into a non-dimensional form. In the CFD Module, streamlines and surface plots are compared with the similarity solution for the magnitude of the velocity, radial velocity, tangential velocity, and axial velocity. The results from the direct simulation in the CFD Module and the solution of dimensionless equations represent a similar solution of velocity distribution. The derived results show that increasing the volume concentration of nanoparticles and effective magnetic parameters decrease the velocity distribution in the flow. Results in the CFD Module are important for monitoring the real-time particle tracing in the flow and, on the other hand, the dimensionless solution is also significant for the physical interpretation of the problem. Both methods of solution empower each other and present the physical model without sacrificing the relevant physical phenomena.

Keywords: nanofluid, velocity, CFD Module, dimensionless analysis

1. INTRODUCTION

Ferrofluids are colloidal suspensions of magnetic nanoparticles. These types of fluid are not present in nature. Ferrofluids are synthesised by different methods based on their application. One of the important properties of ferrofluids is that they work in a zero-gravity region. Ferrofluids have numerous applications in the field of engineering and medicine. Heat control loudspeaker and frictionless sealing are important applications of ferrofluids. However, in the field of medicine, ferrofluid is used in the treatment of cancer through magnetohyperthermia.

The rotational flow of viscous fluid over a rotating disc has been examined by researchers using similarity transformations (Cochran, 1934; Benton, 1966; Schlichting and Gersten, 2017). Based on the models of the rotational flow of viscous fluid, researchers have developed the models for magnetohydrodynamic flow due to rotating disc (Attia, 1998, 2007; Turkyilmazoglu, 2012). Using Rosensweig and Shliomis models, the researchers have demonstrated the flow of ferrofluid due to rotating disc (Ram et al., 2010; 2013a,b). The researchers have investigated the flow over a rotating disc to measure the irreversibility of the system and for heat transfer encampment applications (Qayyum et al., 2018; Rashihi et al., 2013; Hayat et al., 2018). For more practical applications of rotational flow, the researchers have classified the problems pertaining to specific types of nanofluid (Ijaz Khan et al., 2020; Hayay et al., 2017; Mustafa, 2017). Rotating boundary layer flow, flow over a wedge, plate and stagnation point, flow of an electrically conducting fluid along with a vertical plate, and flow over an exponentially accelerated plate have been investigated by researchers and they have presented the similarity solution using numerical techniques (Veera Krishna et al., 2020; Chamkha, 1997; Thameem Basha et al., 2019; Veera Krishna and Chamkha, 2019). However, researchers have demonstrated the perturbation technique to investigate the nanoparticles in blood flow and thermal transport of Williamson nanofluid flow (Bhatti et al., 2020a,b). Abo-Elkhair et al. (2021) used Adomain decomposition method to investigate hybrid bio-nanofluid flow in a peristaltic channel. The researchers have been working continuously to improve the numerical solution of a set of non-dimensional coupled differential of flow over a rotating disc problem (Chaturani and Narasimman, 1991; Rahman, 1978; Schultz and Shah, 1979; Hayat et al., 2018).

Reddy et al. (2017) investigated the flow of Ag-water and Cu-water nanofluids flow due to rotating disc. Takhar et al. (2003) studied the flow of electrically conducting fluid due to a vertical rotating cone and obtained the similarity solution through the finite difference method. Krishana and Chamkha (2020) obtained the analytic solution of the magnetohydrodynamic rotating flow of elastico-viscous fluid. Numerical solutions for the convective flow of nanofluids over a rotating cylinder have been obtained by researchers (Alsabery et al., 2020; Selimefendigil and Chamkha, 2019). Hybrid nanofluid flow in a rotating system, convective flow in a vertical moving cylinder, thin fluid over a vertical plate and conductive fluid over a vertical cone, have been investigated (Kumar et al., 2019; Chmkha et al., 2019; Takhar et al., 2002; Chemkha, 1996). Arain et al. (2020) investigated the multiphase flow between the rotating plates and obtained the numerical solution of similarity equations using the differential transform method. Ali et al. (2021) studied the non-Newtonian Oldroyd-B fluid flow over a parabolic surface and obtained the numerical solution of similarity equations through Runge–Kutta Fehlberg method.

In the present work, the impact of volume concentration and magnetic torque on the swirling flow of water-carrying iron(III)

DOI 10.2478/ama-2021-0016

oxide nanofluid due to the rotating disc is investigated. This swirling flow is considered steady and axisymmetric; therefore, cylindrical equations of the flow are directly numerically solved using the two-dimensional CFD Module in COMSOL Multiphysics. Further, the governing equations are reduced into non-dimensional coupled differential equations using a similarity approach and compared with the results obtained through CFD Module. The similarity model is also validated with the previous theoretical models.

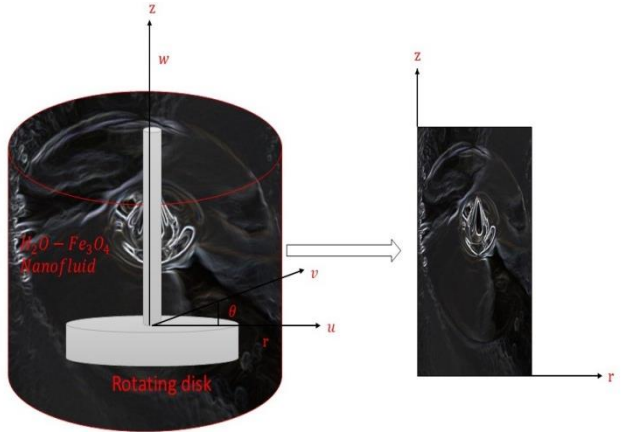

Fig. 1. Flow of axisymmetric nanofluid due to rotating disc and its two-dimensional CFD domain

2. MATHEMATICAL MODEL

The schematic diagram of the flow due to a rotating disc in a tank is shown in Fig. 1. The disc rotates uniformly about the z-axis and generates a three-dimensional boundary layer. The flow is axisymmetric; therefore, the three-dimensional flow has been considered over a two-dimensional region in the CFD Module. The velocities of the water-carrying iron(III) oxide nanofluid changes in the radial and axial directions. In the CFD Module, the computational domain is the two-dimensional geometry (Fig. 1). However, the similarity approach is used on the three-dimensional geometry in Fig. 1. These two approaches of rotational flow for velocity distributions are compared to each other. The flow of magnetic fluid is described by the following equations (Shliomis and Morozov, 1994; Odenbach and Thurm, 2002):

$$\nabla \cdot \boldsymbol{V} = 0 \tag{1}$$

$$\rho_n \left[\frac{\partial \boldsymbol{V}}{\partial t} + (\boldsymbol{V}\cdot\boldsymbol{\nabla})\boldsymbol{V}\right] = -\boldsymbol{\nabla} p + \mu_0 M \boldsymbol{\nabla} H + \mu_n \nabla^2 \boldsymbol{V} + \frac{I}{2\tau_s}\boldsymbol{\nabla} \times \left(\boldsymbol{\omega_p} - \boldsymbol{\Omega}\right) \tag{2}$$

$$I\frac{d\boldsymbol{\omega}_\mathrm{p}}{dt} = \mu_0(\boldsymbol{M}\times\boldsymbol{H}) - \frac{I}{\tau_s}\left(\boldsymbol{\omega}_\mathrm{p} - \boldsymbol{\Omega}\right) \tag{3}$$

The inertial term $\mathrm{I}\frac{\mathrm{d}\omega_\mathrm{p}}{\mathrm{dt}}$ is negligible in comparison with the relaxation term $\mathrm{I}\frac{\omega_\mathrm{p}}{\tau_\mathrm{s}}$. Therefore the equation of rotational motion can be written as (Bacri et al., 1995; Bhabdari, 2020):

$$\boldsymbol{\omega_p} = \boldsymbol{\Omega} + \mu_0 \frac{\tau_s}{I}(\boldsymbol{M}\times\boldsymbol{H}) \tag{4}$$

Using Eq. (4), Eq. (2) can be written as (Shliomis and Morozov, 1994; Bacri et al., 1995):

$$\rho_n \left[\frac{\partial \boldsymbol{V}}{\partial t} + (\boldsymbol{V}\cdot\boldsymbol{\nabla})\boldsymbol{V}\right] = -\boldsymbol{\nabla}\tilde{p} + \mu_n \nabla^2 \boldsymbol{V} + \frac{\mu_0}{2}\boldsymbol{\nabla}\times(\boldsymbol{M}\times\boldsymbol{H}) \tag{5}$$

where $-\nabla\tilde{\mathrm{p}} = -\nabla\mathrm{p} + \mu_0 \mathrm{M}\nabla\mathrm{H}$ denotes the reduced pressure due to magnetisation force [43].

The equilibrium of the magnetic and viscous torque can be written from Eq. (5) as (Ram and Bhandari, 2013; Bacri et al., 1995):

$$\mu_0(\boldsymbol{M}\times\boldsymbol{H}) = -6\mu_n\varphi_1\left(\boldsymbol{\Omega} - \boldsymbol{\omega_p}\right) \tag{6}$$

The Eq. (6) can be written for mean magnetic torque as (Bacri et al., 1995):

$$\mu_0(\overline{\boldsymbol{M}\times\boldsymbol{H}}) = -6\mu_n\varphi_1 m_1 \boldsymbol{\Omega} \tag{7}$$

where m_1 denotes the effective magnetic number due to the applied magnetic field. Using Eqs (6) and (7), the following relation is obtained (Shliomis and Morozov, 1994; Ram and Bhandari, 2013):

$$\frac{\mu_0}{2}\boldsymbol{\nabla}\times(\overline{\boldsymbol{M}\times\boldsymbol{H}}) = \frac{1}{2}\boldsymbol{\nabla}\times -6\mu_n\varphi_1 m_1\boldsymbol{\Omega} \tag{8}$$

$$= -\frac{3}{2}\mu_n\varphi_1 m_1 \boldsymbol{\nabla}(\boldsymbol{\nabla}.\boldsymbol{V}) + \frac{3}{2}\mu_n\varphi_1 m_1 \nabla^2\boldsymbol{v} = \frac{3}{2}\mu_n\varphi_1 m_1 \nabla^2\boldsymbol{V}$$

In the above equation, $\frac{3}{2}\mu_\mathrm{n}\varphi_1\mathrm{m}_1$ is the rotational viscosity due to the applied magnetic field. Using the result in Eq. (8), Eq. (6) can be written as:

$$\rho_n \left[\frac{\partial \boldsymbol{V}}{\partial t} + (\boldsymbol{V}\cdot\boldsymbol{\nabla})\boldsymbol{V}\right] = -\boldsymbol{\nabla}\tilde{p} + \mu_n\left(1 + \frac{3}{2}\varphi_1 m_1\right)\nabla^2\boldsymbol{V} \tag{9}$$

The physical properties of the ferrofluid are as follows (Sheikholeslami and Shehzad, 2018):

$$\rho_n = (1-\varphi_1)\rho_f + \varphi_1\rho_s\,,\quad \mu_n = \frac{\mu_f}{(1-\varphi_1)^{2.5}} \tag{10}$$

The density of the nanofluid depends on the density of the base fluid and volume concentration. Enhancing the concentration of iron(III) oxide increases the density of the nanofluid. Similarly, it changes the viscosity of nanofluids.

Since the flow is considered steady and axisymmetric, Eqs (1) and (9) can be written in cylindrical coordinates as (Shliomis and Morozov, 1994; Bhandari, 2020):

$$\frac{\partial u}{\partial r} + \frac{u}{r} + \frac{\partial w}{\partial z} = 0 \tag{11}$$

$$\rho_n\left[u\frac{\partial u}{\partial r} + w\frac{\partial u}{\partial z} - \frac{v^2}{r}\right] = -\frac{\partial\tilde{p}}{\partial r} + \mu_n\left(1+\frac{3}{2}\varphi_1 m_1\right)\left\{\frac{\partial^2 u}{\partial z^2} + \frac{1}{r}\frac{\partial u}{\partial r} - \frac{u}{r^2} + \frac{\partial^2 u}{\partial r^2}\right\} \tag{12}$$

$$\rho_n\left[u\frac{\partial v}{\partial r} + w\frac{\partial v}{\partial z} + \frac{uv}{r}\right] = \mu_n\left(1+\frac{3}{2}\varphi_1 m_1\right)\left\{\frac{\partial^2 v}{\partial z^2} + \frac{1}{r}\frac{\partial v}{\partial r} + \frac{\partial^2 v}{\partial r^2} - \frac{v}{r^2}\right\} \tag{13}$$

$$\rho_n\left[u\frac{\partial w}{\partial r} + w\frac{\partial w}{\partial z}\right] = -\frac{\partial\tilde{p}}{\partial z} + \mu_n\left(1+\frac{3}{2}\varphi_1 m_1\right)\left\{\frac{\partial^2 w}{\partial z^2} + \frac{1}{r}\frac{\partial w}{\partial r} + \frac{\partial^2 w}{\partial r^2}\right\} \tag{14}$$

The boundary conditions for the considered flow are as follows:

$$z = 0; \quad u = 0,\ v = r\omega,\ \ w = 0;\ z \to \infty\ ;\ \ u \to 0,\ \ v \to 0 \tag{15}$$

In this case, the disc rotates with the uniform angular velocity ω about the axis perpendicular to its plane. No-slip boundary conditions are considered in the flow. The layer of the nanofluid is at the disc which is carried along with the disc. This layer of nanofluid is driven outwards by the centrifugal force. Then new fluid particles are coming towards the disc in the axial direction and these particles are ejected due to centrifugal force. The centrifugal force and radial pressure gradient have an important role in circulating the nanoparticles at a sufficient distance from the wall.

3. NUMERICAL SOLUTION

In the present problem, the swirling flow of water-based Fe_3O_4 nanofluid has been simulated in the CFD 2D axisymmetric module of COMSOL Multiphysics. The following physical parameter has been used in the solution:

Tab. 1. Values of parameters

Parameter	values
ρ_f	997.1[kg m^{-3}]
ρ_s	5500 [kg m^{-3}]
φ_1	0.1
μ_f	0.001[Pa s]
m_1	2
ω	0.5π [rad s^{-1}]

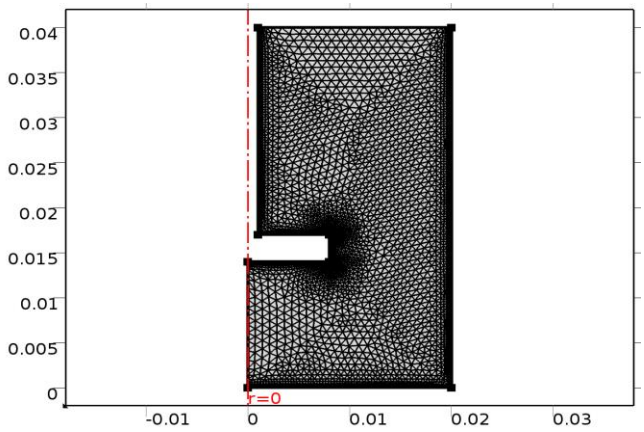

Fig. 2. Mesh selection on the geometry

There are a total of eight boundaries of the domain as shown in Fig. 2. The maximum element size taken is 9×10^{-4} and the minimum size of the element is 4×10^{-5}. The curvature factor selected is 0.3 and the maximum element growth rate is 1.15. The surface plots for the magnitude of the velocity, radial velocity, tangential velocity, axial velocity, and pressure on the nanofluid are presented for different volume fractions and effective magnetic parameters. The values of the parameter used in the solution are given in Tab. 1. In the CFD Module, quadratic interpolation functions are used in the approximation of the solutions. The triangular and quadrilateral elements are used during the solution of the problem. The mesh description of the elements and their properties are shown in Tab. 2. The maximum number of iterations is taken as 300 and the error in the solution is of the order 10^{-5}.

Tab. 2. Mesh description during the finite element method over the domain of the flow

Property	Value
Minimum element quality	0.07274
Average element quality	0.794
Triangular elements	4679
Quadrilateral elements	984
Edge elements	265
Vertex elements	8

Eqs (11)–(15) can also be solved by using similarity transformation. The following similarity transformation has been used to obtain non-dimensional coupled differential equations:

$$u = r\omega E(\alpha), \quad v = r\omega F(\alpha), \quad w = \sqrt{\nu_f \omega}\, G(\alpha),$$
$$\tilde{p} - p_\infty = -\rho\nu\omega P(\alpha),\ \alpha = \sqrt{\frac{\omega}{\nu_f}}z \tag{16}$$

The transformed equations are as follows:

$$\frac{dG}{d\alpha} + 2E = 0 \tag{17}$$

$$\left(1 + \frac{3}{2}\varphi_1 m_1\right)\left[\frac{1}{(1-\varphi_1)^{2.5}\left(1-\varphi_1+\varphi\frac{\rho_S}{\rho_f}\right)}\right]\frac{d^2E}{d\alpha^2} - G\frac{dE}{d\alpha} - E^2 + F^2 = 0 \tag{18}$$

$$\left(1 + \frac{3}{2}\varphi_1 m_1\right)\left[\frac{1}{(1-\varphi_1)^{2.5}\left(1-\varphi_1+\varphi_1\frac{\rho_S}{\rho_f}\right)}\right]\frac{d^2F}{d\alpha^2} - G\frac{dF}{d\alpha} - 2EF = 0 \tag{19}$$

$$\left(1 + \frac{3}{2}\varphi_1 m_1\right)\left[\frac{1}{(1-\varphi_1)^{2.5}\left(1-\varphi_1+\varphi_1\frac{\rho_S}{\rho_f}\right)}\right]\frac{d^2G}{d\alpha^2} - G\frac{dG}{d\alpha} - \frac{dP}{d\alpha} = 0 \tag{20}$$

The boundary conditions are as follows:

$$E(0) = 0, \quad F(0) = 1, \quad G(0) = 0, \quad E(\infty) = 0, \quad F(\infty) = 0 \tag{21}$$

The reduced pressure can be calculated as:

$$P(\alpha) = P_0 + \left(1 + \frac{3}{2}\varphi_1 m_1\right)\left[\frac{1}{(1-\varphi)^{2.5}\left(1-\varphi+\varphi\frac{\rho_S}{\rho_f}\right)}\right]\frac{dG}{d\alpha} - \frac{1}{2}G^2 \tag{22}$$

DOI 10.2478/ama-2021-0016

4. RESULTS AND DISCUSSIONS

In this section, the results ofor radial tangential and axial velocity distribution are presented for different values of volume fraction and effective magnetic parameters. 2D surface plots are obtained from the CFD Module in COMSOL Multiphysics, and for the same problem, a system of nonlinear coupled differential equations has been solved numerically. A brief discussion of the results is presented here.

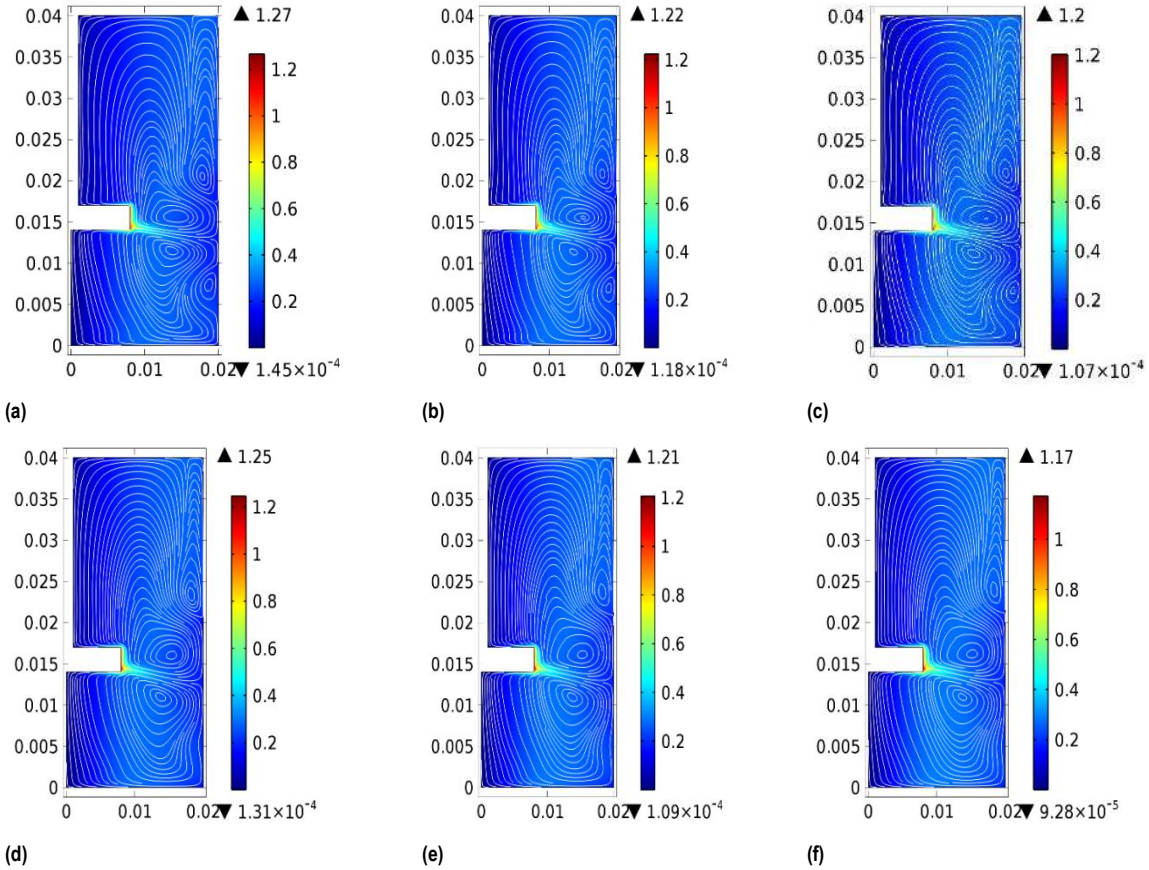

Fig. 3. Surface plot for the magnitude of the velocity (a) $\varphi_1 = 0, m_1 = 2$ (b) $\varphi_1 = 0.2, m_1 = 2$ (c) $\varphi_1 = 0.3, m_1 = 2$ (d) $\varphi_1 = 0.1, m_1 = 2$ (e) $\varphi_1 = 0.1, m_1 = 4$ (f) $\varphi_1 = 0.1, m_1 = 6$

Figs 3(a)–(f) show the magnitude of the velocity for different values of volume concentration and the effective magnetic parameter. Fig. 3(a) shows the magnitude of the velocity of the carrier liquid. Figs 3(b) and 3(c) are obtained for $\varphi_1 = 0.2$ and $\varphi_1 = 0.3$, respectively. It has been shown that for $\varphi_1 = 0.2$ the maximum value of the velocity is 1.22 m/s and for $\varphi_1 = 0.3$ the velocity is 1.20 m/s. Increasing the volume concentration reduces the velocity distribution in the flow. Fig. 3(d) shows the magnitude of the velocity for $m_1 = 2$ and $\varphi_1 = 0.1$. Increasing values of m_1 increases the viscosity of the fluid and therefore reduces the magnitude of the velocity. The velocity is maximum near the rotation of the disc. Similarly, Figs 3(e) and 3(f) are presented for $m_1 = 4$ and $m_1 = 6$, respectively.

Figs 4(a)–(f) show the radial velocity distribution for different values of volume concentration and the effective magnetic parameter. The streamline in the surface plot shows the tangent of the velocity distribution. The radial velocity decreases the increasing values of volume concentration and magnetic parameter. Swirling of the disc in the presence of the magnetic field enhances the difference between the rotation of the particles and fluid. This difference enhances the viscosity of water conveying iron(III) oxide nanofluid. Near the rotating equipment, the velocity is higher than that in other places. Increasing these parameters changes the pattern of streamlines. The velocity changes Fe_3O_4 to become closer than the base fluid. Figs 5(a)–(f) show the tangential velocity distribution for different values of volume concentration and the effective magnetic parameter. The speed of tangential velocity distribution is higher than the radial velocity distribution. When increasing volume concentration and magnetic parameter, the streamlines become closer to each other than in ordinary cases. This situation arises due to the difference in the rotation between the nanoparticles and fluid. The magnetic field increases this misalignment between the rotation of the particles and fluid. Therefore, the viscosity of the nanofluid increases. Figs 6(a)–(f) show the axial velocity distribution for different values of volume concentration and the effective magnetic parameter. Some of the values of the axial velocity are negative. The negative values of the axial velocity show that the flow is directed towards the container.

Fig. 7 shows the magnitude of the dimensionless velocity distribution for different values of φ_1. The magnitude for the velocity in dimensionless form is obtained from the expression $\sqrt{E^2 + F^2 + G^2}$. The velocity distribution is presented on dimensionless axial distance. It is seen that when increasing values of

φ_1, the magnitude of the velocity decreases. The magnitude of the velocity also decreases for increasing values of m_1, as shown in Fig. 8. The results in Figs 7 and 8 represent a similar character as presented in Figs 3(a)–(f). Figs 9 and 10 show the radial velocity distribution for different values of φ_1 and m_1. A case $\varphi_1 = 0$ shows the velocity distribution of the base fluid. Adding Fe_3O_4 nanoparticles with suiTab. surfactants decreases the radial velocity distribution decreases. In the presence of the magnetic field, a decrease in the radial velocity distribution is observed. Figs 11 and 12 show the tangential velocity distribution for different values of φ_1 and m_1. The impact of the volume concentration and rotational viscosity on the tangential velocity distribution is less as compared to radial and axial velocity distributions. Near the surface of the container, the tangential velocity decreases for increasing values of φ_1 and m_1, and far from the surface, these parameters enhance the tangential velocity distribution. Near the surface, the flow of the nanofluid is influenced by the rotating cylinder. Figs 13 and 14 show the axial velocity distribution for different values of φ_1 and m_1. In the absence of magnetic field and iron(III) oxide nanoparticles, the problem reduces to the previous theoretical models of rotational flow. The comparative results with previous theoretical models are shown in Tab. 3. Increasing the values of the volume concentration and effective magnetic parameter decreases the axial velocity. It is noticeable that the physical interpretation of the flow dimensionless approach is very useful and aligned with the results obtained through the CFD Module. However, the CFD Module can provide the problem imagination and more regions for the velocity distribution.

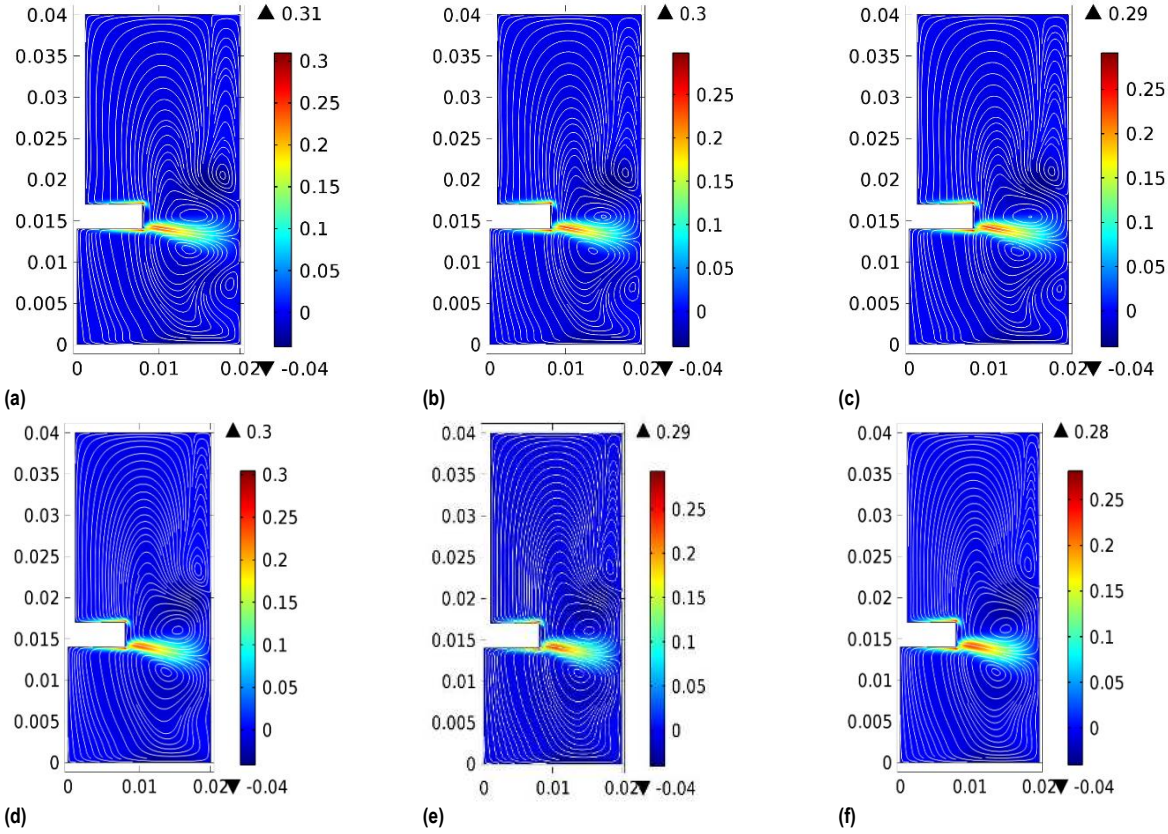

Fig. 4. Surface plot for the radial velocity (a) $\varphi_1 = 0, m_1 = 2$ (b) $\varphi_1 = 0.2, m_1 = 2$ (c) $\varphi_1 = 0.3, m_1 = 2$ (d) $\varphi_1 = 0.1, m_1 = 2$ (e) $\varphi_1 = 0.1, m_1 = 4$ (f) $\varphi_1 = 0.1, m_1 = 6$

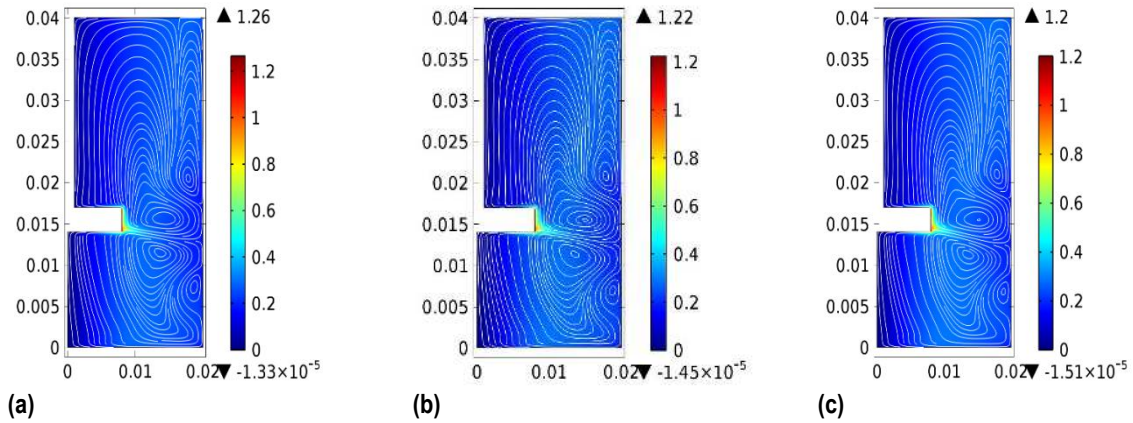

DOI 10.2478/ama-2021-0016

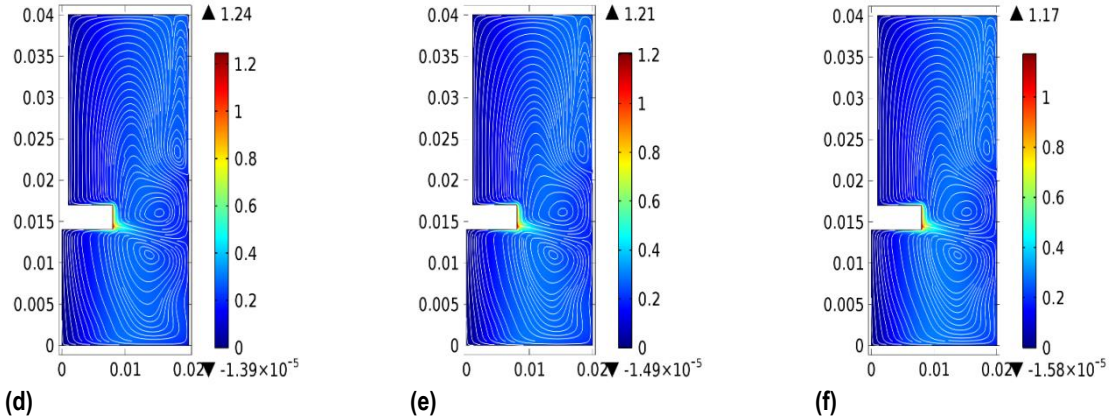

Fig. 5. Surface plot for the tangential velocity (a) $\varphi_1 = 0, m_1 = 2$ (b) $\varphi_1 = 0.2, m_1 = 2$ (c) $\varphi_1 = 0.3, m_1 = 2$ (d) $\varphi_1 = 0.1, m_1 = 2$ (e) $\varphi_1 = 0.1, m_1 = 4$ (f) $\varphi_1 = 0.1, m_1 = 6$

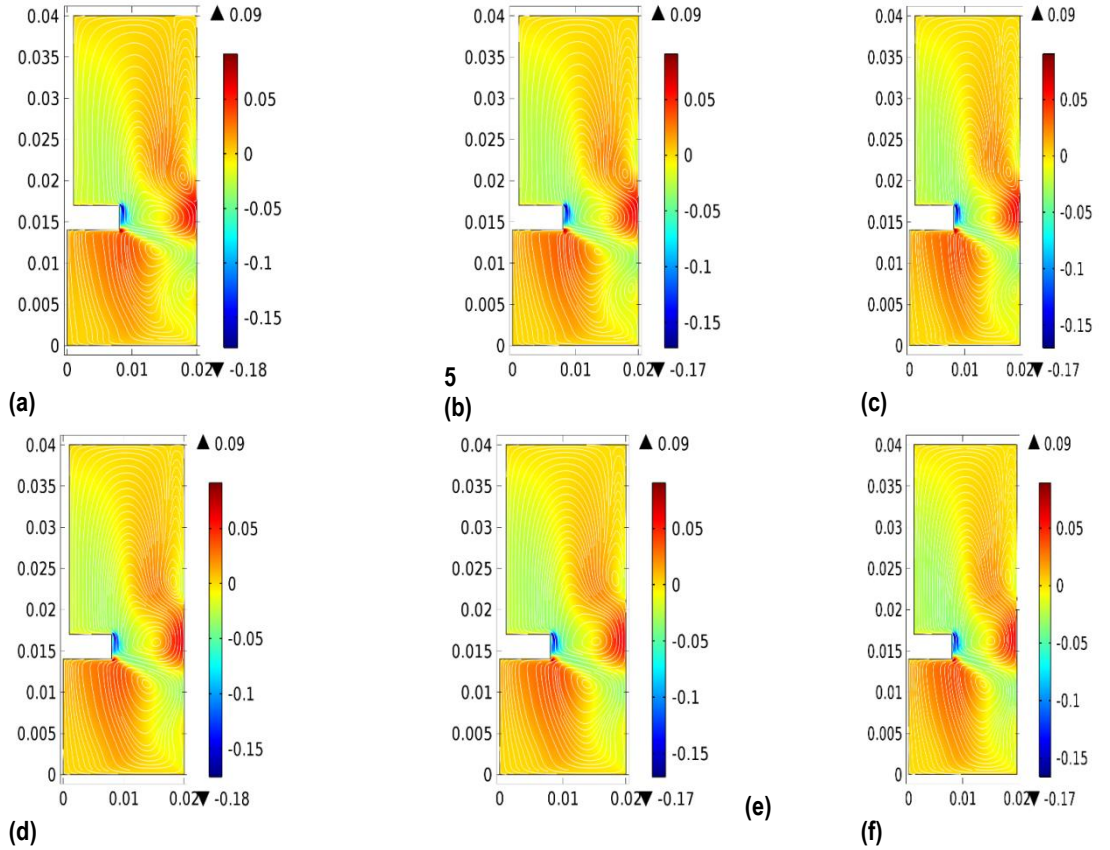

Fig. 6. Surface plot for the axial velocity (a) $\varphi_1 = 0, m_1 = 2$ (b) $\varphi_1 = 0.2, m_1 = 2$ (c) $\varphi_1 = 0.3, m_1 = 2$ (d) $\varphi_1 = 0.1, m_1 = 2$ (e) $\varphi_1 = 0.1, m_1 = 4$ (f) $\varphi_1 = 0.1, m_1 = 6$

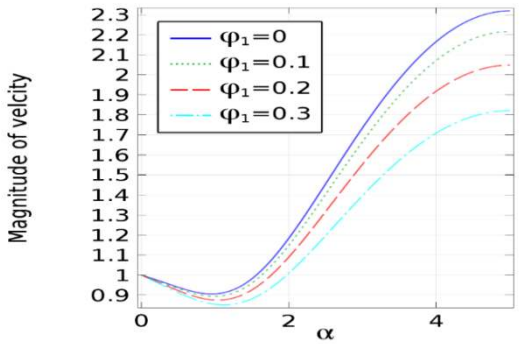

Fig. 7. Magnitude of the velocity for different values of φ_1 at $m_1 = 2$

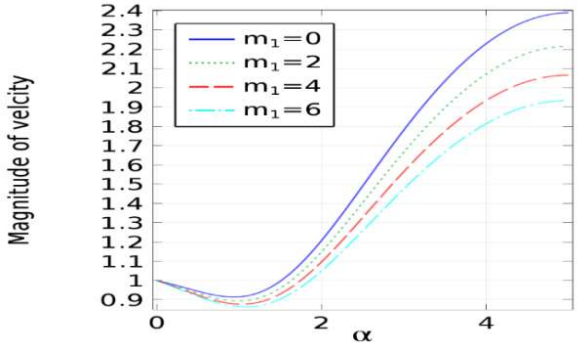

Fig. 8. Magnitude of the velocity for different values of m_1 at $\varphi_1 = 0.1$

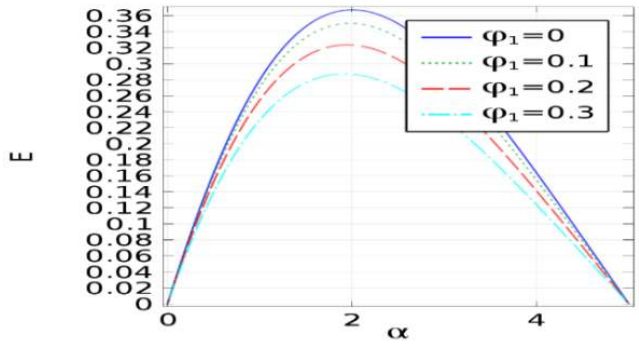

Fig. 9. Radial velocity distribution for different values of φ_1 at $m_1 = 2$

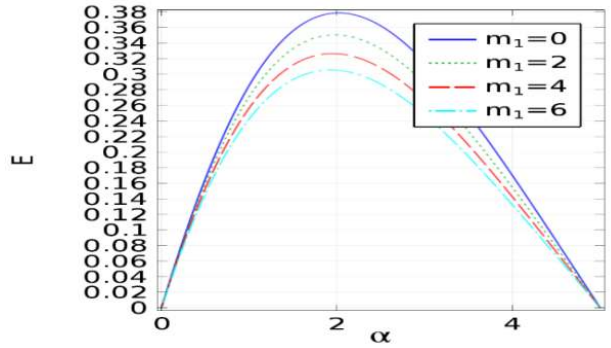

Fig. 10. Radial velocity distribution for different values of m_1 at $\varphi_1 = 0.1$

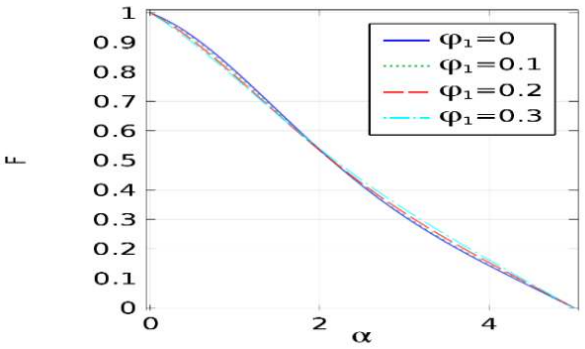

Fig. 11. Tangential velocity distribution for different values of φ_1 at $m_1 = 2$

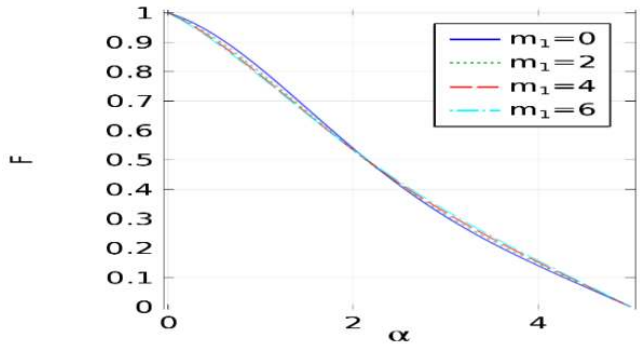

Fig. 12. Tangential distribution for different values of m_1 at $\varphi_1 = 0.1$

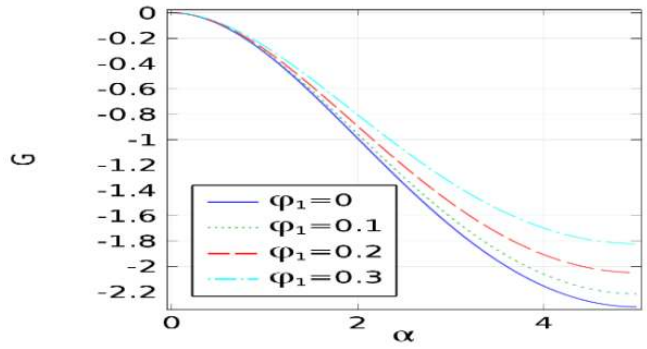

Fig. 13. Axial velocity distribution for different values of φ_1 at $m_1 = 2$

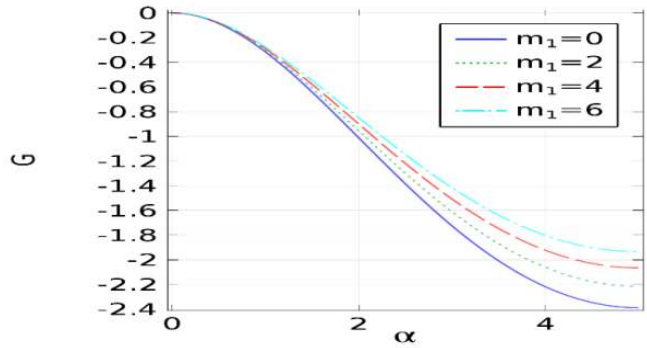

Fig. 14: Axial velocity distribution for different values of m_1 at $\varphi_1 = 0.1$

Tab. 3. Comparison of similarity solution with previous theoretical models for $\varphi_1 = \mathrm{m}_1 = 0$

	$E'(0)$	$F'(0)$
Kelson and Desseaux [47]	0.510233	-0.615922
Bachok et al. [48]	0.5102	-0.6159
Turkyilmazoglu [49]	0.51023262	-0.61592201
Present Result	0.5102337	-0.6159241

5. CONCLUSIONS

The swirling flow of water-based Fe_3O_4 nanofluid with different volume concentrations and rotational viscosity has been studied. The results for the velocity distribution have been obtained through the CFD Module and dimensional analysis. These results indicate that increasing the volume concentration and rotational viscosity decreases the velocity distribution. These results show the comparative results between the CFD Module and dimensionless analysis. Both techniques favour the findings of each other. For the physical interpretation of the results, dimensionless analysis is important. However, for real-time particle tracing CFD Module is important. These results show that both types of studies are relevant to the development of swirling flow analysis. These results might be useful in bringing about an improvement in the sealing of hard disc drives.

Nomenclature:

E	Dimensionless component of radial velocity
F	Dimensionless component of tangential velocity
G	Dimensionless component of axial velocity
$\boldsymbol{H}$	Magnetic field intensity (A/m)

I	Sum of the particles moment of inertia (kg/m^2)
$\boldsymbol{M}$	Magnetization (A/m)
m_1	Effective magnetic parameter
p	Fluid Pressure (kg/m/s^2)
$\tilde{p}$	Reduced fluid pressure (kg/m/s^2)
r	Radial direction (m)
t	Time (s)
u	Radial velocity (m/s)
v	Tangential velocity $(\mathrm{m/s})$
$\boldsymbol{V}$	Velocity of ferrofluid $(\mathrm{m/s})$
w	Axial velocity (m/s)
z	Axial direction (m)
ρ_n	Nanofluid density (kg/m^3)
ρ_f	Carrier liquid density (kg/m^3)
ρ_s	Nanoparticles density (kg/m^3)
μ_0	The magnetic permeability of free space (H/m)
μ_n	Reference viscosity of nanofluid $(\mathrm{kg/m/s2})$
μ_n	Reference viscosity of carrier liquid (kg/m/s^2)
ν_f	Kinematic viscosity of the base fluid (m^2/s)
∇	Gradient operator $(/\mathrm{m})$
τ_s	Rotational relaxation time (/s)
ω_p	Angular velocity of particles $(\mathrm{rad/s})$
Ω	Vorticity $(\mathrm{rad/s})$
ω	Angular velocity $(\mathrm{rad/s})$
θ	Tangential direction (rad)
φ_1	Volume concentration
ν_n	Kinematic viscosity without magnetic field (m^2/2)
α	Dimensionless distance parameter

REFERENCES

1. **Abo-Elkhair R.E., Bhatti M.M., Mekheimer K.S.** (2021), Magnetic force effects on peristaltic transport of hybrid bio-nanofluid (Au–Cu nanoparticles) with moderate Reynolds number: An expanding horizon, *Int. Commun. Heat Mass Transf.*, 123, 105228.
2. **Ali Z., Zeeshan A, Bhatti M.M., Hobiny A., Saeed T.** (2021), Insight into the Dynamics of Oldroyd-B Fluid Over an Upper Horizontal Surface of a Paraboloid of Revolution Subject to Chemical Reaction Dependent on the First-Order Activation Energy, *Arab. J. Sci. Eng.,* 1–10.
3. **Alsabery A.I., Ghalambaz M., Armaghani T., Chamkha, I. Hashim I., Pour M.S.** (2020), Role of rotating cylinder toward mixed convection inside a wavy heated cavity via two-phase nanofluid concept, *Nanomaterials*, 10(6), 1–22.
4. **Arain M.B, Bhatti M.M., Zeeshan A., Saeed T., Hobiny A.** (2020), Analysis of arrhenius kinetics on multiphase flow between a pair of rotating circular plates, *Math. Probl. Eng.*, 2020.
5. **Attia H.A** (1998), Unsteady MHD flow near a rotating porous disk with uniform suction or injection, *Fluid Dyn. Res.*, 23(5), 283–290.
6. **Attia H.A.** (2007), On the effectivness of ion slip and and uniform suction or injection on steady MHD flow due to rotating disk with heat transfer ohmic heating, *Chem. Eng. Commun.*, 194(10), 1396–1407.
7. **Bachok N., Ishak A., Pop I.** (2011), Flow and heat transfer over a rotating porous disk in a nanofluid, *Phys. B Phys. Condens. Matter*, 406(9), 1767–1772.
8. **Bacri J.C., Perzynski R., Shliomis M.I., Burde G.I.** (1995), Negative-viscosity effect in a magnetic fluid, *Phys. Rev. Lett.*, 75(11), 2128–2131.
9. **Benton E.R.** (1966), On the flow due to a rotating disk, *J. Fluid Mech.*, 24(4), 781–800.
10. **Bhandari A.** (2020a), Study of ferrofluid flow in a rotating system through mathematical modeling, *Math. Comput. Simul.*, 178, 290–306.
11. **Bhandari A.** (2020b), Study of magnetoviscous effects on ferrofluid flow, *Eur. Phys. J. Plus*, 135(7), 537.
12. **Bhatti M.M, Marin M., Zeeshan A., Ellahi R., Abdelsalam S.I.** (2020a), Swimming of motile gyrotactic microorganisms and nanoparticles in blood flow through anisotropically tapered arteries, *Front. Phys.*, 8(95).
13. **Bhatti M.M., Riaz A., Zhang L., Sait S.M., Ellahi R.** (2020b), Biologically inspired thermal transport on the rheology of Williamson hydromagnetic nanofluid flow with convection: an entropy analysis, *J. Therm. Anal. Calorim.*, 1–16.
14. **Chamkha A.J.** (1996), Non-darcy hydromagnetic free convection from a cone and a wedge in porous media, *Int. Commun. Heat Mass Transf.*, 23(6), 875–887.
15. **Chamkha A.J.** (1997), MHD-free convection from a vertical plate embedded in a thermally stratified porous medium with Hall effects, *Appl. Math. Model.*, 21(10), 603–609.
16. **Chamkha A.J., Dogonchi A.S., Ganji D.D.** (2019), Magneto-hydrodynamic flow and heat transfer of a hybrid nanofluid in a rotating system among two surfaces in the presence of thermal radiation and Joule heating, *AIP Adv.*, 9(2), 025103.
17. **Chaturani P., Narasimman S.** (1991), Numerical solution of a micropolar fluid flow between two rotating coaxial disks, *Acta Mech.*, 89(1-4), 133–145.
18. **Cochran W.G.** (1934), The flow due to a rotating disc, *Math. Proc. Cambridge Philos. Soc.*, 30(3), 365–375.
19. **Hayat T., Aziz A., Muhammad T., Alsaedi A**. (2018a), Numerical treatment for Darcy–Forchheimer flow of nanofluid due to a rotating disk with convective heat and mass conditions, *Int. J. Numer. Methods Heat Fluid Flow*, 28(11), 2531–2550.
20. **Hayat T., Qayyum S., Khan M.I., Alsaedi A.** (2018b), Entropy generation in magnetohydrodynamic radiative flow due to rotating disk in presence of viscous dissipation and Joule heating, *Phys. Fluids*, 30(1), 017101.
21. **Hayat T., Rashid M., Imtiaz M., Alsaedi A.** (2017), Nanofluid flow due to rotating disk with variable thickness and homogeneous-heterogeneous reactions, *Int. J. Heat Mass Transf.*, 113, 96–105.
22. **Ijaz Khan M., Khan S.A., Hayat T., Imran Khan M., Alsaedi A.** (2020), Entropy optimization analysis in MHD nanomaterials (TiO2-GO) flow with homogeneous and heterogeneous reactions, *Comput. Methods Programs Biomed.*, 184.
23. **Kelson N., Desseaux A.** (2000), Note on porous rotating disk flow, *ANZIAM J.*, 42, 837.
24. **Krishna M.V., Chamkha A.J.** (2020), Hall and ion slip effects on MHD rotating flow of elastico-viscous fluid through porous medium, *Int. Commun. Heat Mass Transf.*, 113, 104494.
25. **Kumar B., Seth G.D., Nandkeolyar R., Chamkha A.J.** (2019), Outlining the impact of induced magnetic field and thermal radiation on magneto-convection flow of dissipative fluid, *Int. J. Therm. Sci.*, 146, 106101.
26. **Mustafa M.** (2017), MHD nanofluid flow over a rotating disk with partial slip effects: Buongiorno model, *Int. J. Heat Mass Transf.*, 108, 1910–1916.
27. **Odenbach S., Thurm S.** (2002), *Magnetoviscous Effects in Ferro-fluids*, 185–201.
28. **Qayyum S., Hayat T., Khan M.I., Alsaedi A.** (2018), Optimization of entropy generation and dissipative nonlinear radiative Von Karman's swirling flow with Soret and Dufour effects, *J. Mol. Liq.,* 262, 261–274.
29. **Rahman M.** (1978), On the numerical solution of the flow between a rotating and a stationary disk, *J. Comput. Appl. Math.*, 4(4), 289–293.
30. **Ram P., Bhandari A.** (2013a), Effect of phase difference between highly oscillating magnetic field and magnetization on the unsteady ferrofluid flow due to a rotating disk, *Results Phys.*, 3, 55–60.
31. **Ram P., Bhandari A.** (2013b), Effect of phase difference between highly oscillating magnetic field and magnetization on the unsteady ferrofluid flow due to a rotating disk, *Results Phys.,* 3, 55–60.
32. **Ram P., Bhandari A**. (2013c), Negative viscosity effects on ferrofluid flow due to a rotating disk, *Int. J. Appl. Electromagn. Mech.*, 41(4), 467–478.

33. **Ram P., Sharma K., Bhandari A.** (2010), Effect of Porosity on Ferrofluid Flow With Rotating Disk, 6(16), 67–76.
34. **Rashidi M.M., Abelman S., Mehr N.F.** (2013), Entropy generation in steady MHD flow due to a rotating porous disk in a nanofluid, *Int. J. Heat Mass Transf.*, 62(1), 515–525.
35. **Reddy P.S., Sreedevi P., Chamkha A.J.** (2017), MHD boundary layer flow, heat and mass transfer analysis over a rotating disk through porous medium saturated by Cu-water and Ag-water nanofluid with chemical reaction, *Powder Technol.*, 307, 46–55.
36. **Rosensweig R.E.** (1997), *Ferrohydrodynamics,* Dover Publications.
37. **Schlichting H., Gersten K.** (2017), *Boundary-Layer Theor*, Berlin, Heidelberg: Springer Berlin Heidelberg.
38. **Schultz D.H., Shah V.L.** (1979), Numerical solution of laminar recirculating flow between shrouded rotating disks, *Comput. Fluids*, 7(2), 137–144.
39. **Selimefendigil F., Chamkha A.J.** (2019), MHD mixed convection of nanofluid in a three-dimensional vented cavity with surface corrugation and inner rotating cylinder, *Int. J. Numer. Methods Heat Fluid Flow*, 30(4), 1637–1660.
40. **Sheikholeslami M., Shehzad S.A.** (2018), Numerical analysis of Fe3O4–H2O nanofluid flow in permeable media under the effect of external magnetic source, *Int. J. Heat Mass Transf.*, 118, 182–192.
41. **Shliomis M.I., Morozov K.I.** (1994), Negative viscosity of ferrofluid under alternating magnetic field, Phys. Fluids, 6(8), 2855–2861.
42. **Takhar H.S., Chamkha A.J., Nath G.** (2002), Combined heat and mass transfer along a vertical moving cylinder with a free stream, *Heat Mass Transf.*, 36(3), 237–246.
43. **Takhar H.S., Chamkha A.J., Nath G.** (2003), Unsteady mixed convection flow from a rotating vertical cone with a magnetic field, *Heat Mass Transf. und Stoffuebertragung*, 39(4), 297–304.
44. **Thameem Basha H., Sivaraj R., Subramanyam Reddy A., Chamkha A.J.** (2019), SWCNH/diamond-ethylene glycol nanofluid flow over a wedge, plate and stagnation point with induced magnetic field and nonlinear radiation – solar energy application, *Eur. Phys. J. Spec. Top.*, 228(12), 2531–2551.
45. **Turkyilmazoglu M.** (2012), MHD fluid flow and heat transfer due to a stretching rotating disk, *Int. J. Therm. Sci.*, 51(1), 195–201.
46. **Turkyilmazoglu M.** (2014), Nanofluid flow and heat transfer due to a rotating disk, *Comput. Fluids*, 94, 139–146.
47. **Veera Krishna M., Ameer Ahamad N., Chamkha A.J.** (2020), Hall and ion slip effects on unsteady MHD free convective rotating flow through a saturated porous medium over an exponential accelerated plate, *Alexandria Eng. J.*, 59(2), 565–577.
48. **Veera Krishna M., Chamkha A.J. (**2019), Hall and ion slip effects on MHD rotating boundary layer flow of nanofluid past an infinite vertical plate embedded in a porous medium, *Results Phys.*, 15, 102652.

Anupam Bhandari: https://orcid.org/0000-0002-2881-0078